Journal Pre-proofs

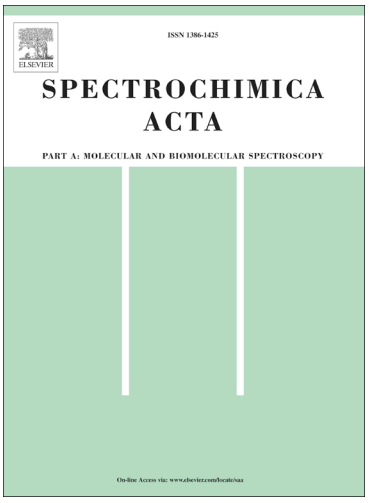

Multiframe-based non-local means denoising for Raman spectra

Zhen Liu, Mohamed A. Ettabib, Bethany M. Bowden, Philip N. Bartlett, James S. Wilkinson, Michalis N. Zervas

PII: S1386-1425(24)00097-0
DOI: https://doi.org/10.1016/j.saa.2024.123931
Reference: SAA 123931

To appear in: *Spectrochimica Acta Part A: Molecular and Biomolecular Spectroscopy*

Received Date: 6 June 2023
Revised Date: 17 January 2024
Accepted Date: 19 January 2024

Please cite this article as: Z. Liu, M.A. Ettabib, B.M. Bowden, P.N. Bartlett, J.S. Wilkinson, M.N. Zervas, Multiframe-based non-local means denoising for Raman spectra, *Spectrochimica Acta Part A: Molecular and Biomolecular Spectroscopy* (2024), doi: https://doi.org/10.1016/j.saa.2024.123931

Multiframe-based non-local means denoising for Raman spectra

Zhen Liu[1*], Mohamed A. Ettabib[1], Bethany M. Bowden[2], Philip N. Bartlett[2], James S. Wilkinson[1], Michalis N. Zervas[1]

[1]Zepler Institute for Photonics and Nanoelectronics, University of Southampton, Southampton SO17 1BJ, United Kingdom

[2]School of Chemistry, University of Southampton, Southampton SO17 1BJ, United Kingdom

*Corresponding author: zhen.liu@soton.ac.uk

Abstract

A method for denoising Raman spectra is presented in this paper. The approach is based on the principle that the original signal can be restored by averaging pixels based on structure similarity. Similarity searching and averaging are not limited to the neighbouring pixels but extended throughout the entire signal range across different frames. This approach is distinguished from the conventional single-frame neighbour pixel-based filtering. The effectiveness and robustness of the proposed method are demonstrated through denoising simulated and experimental Raman data sets with fixed denoising parameters. Several denoised results and statistical indicators are presented for the simulated data. Recovery of the experimental Raman spectrum from our newly developed cost-effective waveguide-enhanced Raman spectroscopy system is also presented and compared to the spectrum from a conventional expensive Raman microscope for the same analyte.

Keywords: Spectra restoration, Non-local means, Multi-frame denoising, Waveguide enhanced Raman spectroscopy

The manuscript

1. Introduction

Raman spectroscopy is a powerful technique for analysing the structure and composition of materials. However, the Raman signal is usually weak and, due to its small excitation and emission cross-section, is often obscured by background noise generated by various sources [1,2]. Thus, denoising is crucial for extracting reliable and informative data from raw Raman spectra.

Common denoising methods, including low-pass filtering and median filtering in both the space and frequency domains, are typically applied to remove noise [1]. Among these simple filters, Gaussian filtering and median filtering are commonly used in most denoising scenarios, including Raman spectra denoising, and often act as baseline techniques to characterize new denoising methods [3]. These filtering techniques, however, have a smoothing effect on the data that can suppress random fluctuations but may result in a loss of contrast between signal and noise, flattening the Raman peaks in the signal, and thereby reducing the effectiveness of the denoising process [1]. Advanced methods, such as the Savitzky-Golay (SG) filter [4], which is based on polynomial fitting, and the wavelet method [5], which is based on frequency filtering, have been adapted and applied to processing Raman spectra. The SG filter method has shown good performance but can potentially remove genuine Raman peaks with low full width at half maximum (FWHM) if the parameters are not appropriately set [1]. As to the fitting-based method, complicated (pre-) processing, such as feature extraction [6] and even computation-cost deep learning [7], were proposed to improve the performance of fitting and to reduce signal distortion for denoising the spectra. The wavelet transform filtering (WTF) method provides more discriminating frequency filtering than a simple Fourier transform because of multiscale frequency decomposition, so more precise denoising can be achieved than the typical low-pass filtering via Fourier transform in the frequency domain. However, sensitive thresholds for every decomposed frequency component have to be set. In addition, proper wavelets need to be chosen from the large family of wavelets, and complicated optimization algorithms[8] have been developed just for choosing appropriate parameters for WTF. More recently, WTF is also reported to be integrated with machine learning algorithms to increase the robustness of WTF for pre-processing the Raman spectra [9]. Such sensitive and complicated parameter settings can be a challenging task for non-expert users, which limits their applicability in practice and potential for fully automated Raman signal processing.

In contrast to all the aforementioned current neighbour-pixel-based filtering methods, the non-local means (NLM) in 2005 [10] provided new thoughts in the field of image restoration. It extracts signals by comparing the similarity of the pixel patch across the whole image and replacing the pixels with similarity-weighted averaging. NLM has demonstrated effective performance in noise reduction without complicated multi-parameter settings. It has been described as “parameter-free” [11] and is known for its ability to preserve high-frequency signals while cancelling out noise in the same high-frequency domain, thus acting as an "edge-preserving denoising method" [12]. Recently,

the NLM has also been successfully applied to a periodic signal for fault diagnosis of rolling bearings [13].

In this paper, inspired by NLM, we propose, explore and implement a new algorithm, the multi-frame NLM (MNLM) based method, to address current challenges for Raman signal denoising. In practice, the Raman spectrum for a specific analyte can be easily acquired multiple times, and each frame of the spectrum is identical but polluted with random noise. We assume that the noise pattern in different frames acquired from the spectrometer with the same acquisition parameters is similar. Therefore, we expect that the signal can be restored by averaging the pixel blocks across the entire signal range in different frames based on similarity. MNLM is expected to preserve the outstanding features of NLM, such as "edge-preserving" and "parameter-free" to address the weaknesses of current denoising methods for Raman spectra.

Following the description of the MNLM in section 2, a thorough three-phase validation, covering simulated and experimental data, is introduced and conducted in section 3. Following the common practice of validating denoising algorithms [10,14,15], our first-phase and second-phase validations employ artificial Gaussian noise for presenting statistical quantitative indicators. In addition to the conventional validation approaches, and to avoid using any artificial data, the third-phase validation that involves deconvolution is introduced. Deconvolution is a low-cost computational ill-conditioned post-processing technique to increase the resolution of a physical instrument but sensitively relies on the quality of the input. Therefore, beyond the conventional practice of quantitative validation on denoising algorithms with artificially degraded signals, in the third phase of validation, MNLM is exploited as a pre-processing step for the deconvolution applied to our experimental spectra from our low-cost waveguide enhanced Raman spectroscopy (WERS) system [16] to further demonstrate its accuracy and efficacy.

2. Algorithms and implementation

MNLM is demonstrated to restore the Raman signal that is degraded by additive noise, expressed as follows

$$\boldsymbol{Y}(\boldsymbol{i},\boldsymbol{j}) = \boldsymbol{X}(\boldsymbol{i},\boldsymbol{j}) + \boldsymbol{n}(\boldsymbol{i},\boldsymbol{j}), \tag{1}$$

$\boldsymbol{Y} = \{y_i^T \mid i \in N\}$is the 2D matrix of raw data, consisting of N frames spectra in a 1D vector, where $y_i = \{y(j) \mid j \in V\}$ is the i^{th} frame Raman spectrum sub-vector, and $\boldsymbol{Y}(i,j)$ is the observed signal at j^{th} position in i^{th} frame. $\boldsymbol{X}$ is the unpolluted original signal and n is the additive noise.

Similarly, to standard NLM, the MNLM filter recovers the estimated signal $\hat{x}$ by weighted averaging of all pixel values in the searching window. However, unlike standard NLM used in imaging, in MNLM, the searching window is extended to other frames that are sampled with the same acquisition parameters, and the weight for averaging is calculated based on the 1D sub-vectors as shown in Fig. 1 (it is worth noting that the

calculation in standard NLM is performed on 2D sub-matrices. The recovered j_1^{th} pixel block in i_1^{th} frame is expressed as

$$\hat{x}_{i_1}(j_1) = \sum_{j_2 \in V} \sum_{i_2 \in V} \omega_{i_1,j_1}(i_2, j_2)\, y_{i_2}(j_2), \tag{2}$$

where $\omega_{i_1,j_1}(i_2,j_2)$is the normalized weight, and the value is determined by the similarity between the j_1^{th} pixel block M_{j_1}, i.e. $y_{i_1}(M_{j_1}) = \{y(j) | j \in M_{j_1}\}$, in i_1^{th} frame and the j_2^{th} pixel block M_{j_2}in the i_2^{th} frame. The similarity between $M_{j_1}$and M_{j_2} is measured by the Gaussian-weighted Euclidean distance between the two vectors, namely,

$$d^2_{i_1,j_1}(i_2, j_2) = \| y_{i_1}(M_{j_1}) - y_{i_2}(M_{j_2}) \|^2_{2,a}, \tag{3}$$

the operator $\| * \|^2_{2,a}$ denotes L^2 norm with Gaussian convolution. Here a is the standard deviation of the Gaussian kernel, i.e., $\| y \|^2_{2,a} = \| y \otimes G_a \|^2_2$, where the symbol $\otimes$ represents the convolution operator. The concept of using L^2 norm with Gaussian convolution to calculate the Gaussian-weighted Euclidean distance instead of using L^2 norm to calculate the Euclidean distance with standard Gaussian kernel (where the standard deviation a is 1) aligns with the foundation approach of NLM in Ref. [10] and [17]. The purpose of applying Gaussian weighting to the Euclidean distance between the two vectors is to emphasize the significance of the central pixel in the neighbourhood. As the similarity between the neighbourhoods $M_{j_1}$and M_{j_2} increases, the Gaussian-weighted Euclidean distance $d_{i_1,j_1}(i_2,j_2)$ between the corresponding vectors $y_{i_1}(M_{j_1})$ and $y_{i_2}(M_{j_2})$ decreases, resulting in a higher weight of a pixel $j_1$during the calculation of the average value

$$\omega_{i_1,j_1}(i_2, j_2) = \frac{1}{Z_{i_1,j_1}} e^{-\frac{d^2_{i_1,j_1}(i_2,j_2)}{h^2}}, \tag{4}$$

where $Z_{i_1,j_1}$is a normalization parameter to ensure $\Sigma \omega_{i_1,j_1} = 1$, and h is the smoothing factor. As established in Ref. [17], the smoothing factor is linearly related to the standard deviation of noise, σ_n, in NLM, and expressed as $h = k\sigma_n$, where the typical k value is around 0.5 for optimal denoising performance in the case that the σ_n is known or can be well estimated. However, as an important parameter, the choice of the value of smoothing factor is discussed in the parameter-sweeping Section.

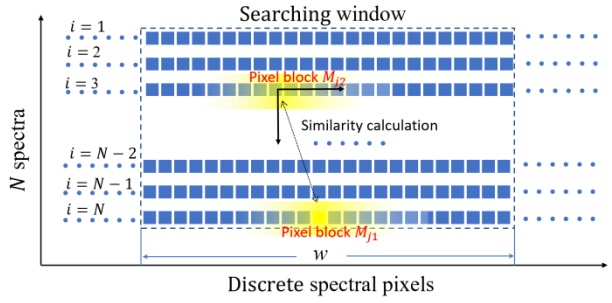

Fig. 1. Diagram of MNLM searching performed on N spectra. The Gaussian-weighted Euclidean distance between the two pixel-blocks is calculated in the whole searching window in N frames with width of w.

The key function of the algorithm is in calculating the weights for each pixel, which depend on the similarity calculated by Gaussian-weighted Euclidean distance in Eqn. (3). Fig. 1 illustrates the processing of searching similarity between each two pixel-blocks within a designed searching window. The searching window has a size of $w \times N$,where w is the user defined width of the searching window and N is the total frame number. The searching window confines the disparity of the pixel count between the centres of the two blocks, $M_{j_1}$and M_{j_2} in Eqn. (3), to be less than $w/2$.

With the Gaussian-weighted Euclidean distance calculated via Eqn. (3), the weights for each pixel are obtained with Eqn. (4). Subsequently, the pixel value is reconstructed through weighted averaging of all the pixels in the searching window across different N frames, utilizing Eqn. (2). Finally, the true value of signal, $\boldsymbol{X}$ in Eqn. (1) is approached with $\hat{\boldsymbol{X}}$ by applying Eqn. (2) to all the pixels within the whole signal frame.

After elucidating the mechanism of the algorithm, it is worth noting that the searching window width w serves as another denoising parameter. It is discussed in parameter-sweeping section, alongside the smoothing factor, for optimal denoising performance. The implementation is conducted with the free-license Python package *SciPy* [18].

3. Validation

To thoroughly validate the effectiveness, robustness and the generalization ability, the validation of our MNLM involves three different phases of spectra sources. These sources encompass the simulated Raman spectra dataset, experimental Raman spectra dataset and Raman spectra for the same analyte from different spectroscopy systems.

To obtain accurate statistical indicators for the processing quality, the denoised spectra must be compared to the “real” spectra to conduct the calculation, while the “real” Raman spectra would be degraded by inherent experimental factors, acquisition due to the extremely small cross-section and various sources of noise. To address this issue, a group of simulated Raman spectra is employed as the reference "real" spectra for the first phase dataset. These simulated spectra are devoid of noise, and then artificial noise is added to simulate the degradation that experimental acquisition would introduce. The procedure to generate simulated Raman spectra is specified at the beginning of Section 3.1. The MNLM is applied to the simulated degraded Raman spectra for restoration. With the known “real” spectra and recovered spectra, it is straightforward to calculate the indicators characterizing the effectiveness of the restoration.

However, it is important to acknowledge that the experimental spectra are more complicated than the simulated spectra in practice, which might possibly diminish the effectiveness of the denoising processing. To account for this complexity, the second-phase validation is conducted with the experimental spectra dataset sourced from the RRUFF project [19]. The RRUFF project provides high-quality Raman spectra for well

characterized minerals collected from research groups across the world. The spectra dataset from RRUFF serves as the baseline "real" spectra for calculating the indicators, although the imperfections of the experimental spectra could slightly affect the accuracy when calculating the indicators. Artificial noise is introduced to degrade the RRUFF spectra, which are subsequently subjected to restoration using our MNLM method. The statistical indicators are then computed with the restored and original RRUFF spectra. The experimental Raman spectra dataset, consisting of 40 frames experimental Raman spectra that were submitted to RRUFF project by various research groups, is utilized to validify our MNLM. This dataset is also deposited in supporting dataset [20]. This stage enables the validation with experimental data for the effectiveness as well as the generalization ability, i.e., our method can work for the spectra from various sources.

To eliminate the use of any artificial signals or artificial noise, the third phase of validation exclusively relies on experimental data, although in this case the "real" signal for computing indicators will not be precisely obtained. However, instead of presenting indicators, the MNLM is validated by serving as a pre-processing step for deconvolution. It is well known that deconvolution is ill-conditioned and is sensitive to any noise and inaccurate preprocessing. Therefore, successful deconvolution after MNLM denoising would confirm the accuracy and efficacy of the MNLM. The last phase of validation involves the spectra acquired from the expensive conventional Raman microscope and our low-cost waveguide enhanced Raman spectroscopy (WERS) system [16] both for the same analytes. The WERS spectra are processed with our MNLM and the baseline denoising methods. The processed spectra are then compared to the spectra from a Raman microscope. The indicators are not shown at this point as the form of spectra from the Raman microscope is different to that of WERS spectra. Different instrument function, wavelength distortion, polarization effects and other factors mean that the Raman microscope spectra cannot be considered as an appropriate reference against the WERS spectrum to calculate the indicators accurately. However, the effectiveness of our MNLM in enhancing our low-cost WERS system is evident through direct spectral comparisons.

Section 3.1, 3.2 and 3.3 rely on the data prepared in the first phase and second phase validations. Following demonstration of the effectiveness of involving multiple frame spectra for denoising in section 3.1, and weak sensitivity to denoising parameters in section 3.2, the quality of processed spectra is demonstrated in section 3.3 using classical quantitative indicators computed with large-size datasets. The third phase validation, which relies on our experimental data, is presented in section 3.4.

3.1. Validations with simulated and experimental data

To validate the algorithm, an artificial Raman spectrum is generated by applying the following procedure. A frame of Raman spectrum is simulated with multiple Lorentz peaks, as usually utilized for Raman peak fitting [21]. Each frame contains 1000 data points, including random 7-15 Lorentzian peaks with random positions, random heights within 0 to 1, and random half-widths between 1 and 7 pixels. The noise is an artificially generated random matrix with a size of $N \times 1000$, namely N frame noise vectors. Each signal vector is added with random vectors in the noise matrix to obtain N frames data set, simulating N frames of noisy Raman signal acquired from the same spectrometer. This procedure has

been repeated 30 times, so a dataset with $N \times 30$ frames of the simulated signal is prepared for validating the algorithm.

To start the validation process, the standard deviation, σ_n, of the random matrix is set to 0.05. A 5-frame averaged original, degraded, MNLM processed signal is shown in Fig. 2 (I). The Gaussian filtering and median filtering as the two standard denoising approaches are also conducted for comparison. The results show that the fine structure of the original signal, e.g., the overlapping double-peaks around 50, 420 and 750 are preserved by all the methods, however, the MNLM method shows evidence of a much better performance in removing noise without over flattening the signal peaks (e.g., the main peak at 420).

In addition to simulated spectra, the same processing has been applied to the experimental spectra of aegirine from the RRUFF project [19]. Each RRUFF spectrum is added to N frame artificial noise vectors, followed by denoising procedures. The set of original, degraded and processed spectra for aegirine from the RRUFF project is displayed in Fig. 2 (II). As in the simulated spectra set, the fine structures of the original spectrum, e.g., multi-peaks around 300 cm^{-1}, have been preserved by all methods, while the MNLM shows much better ability at precisely restoring the signal peaks without over flattening (e.g., the main peak at 200 cm^{-1}).

The superior performance on denoising both simulated and experimental spectra will be quantified with indicators in the following Sections.

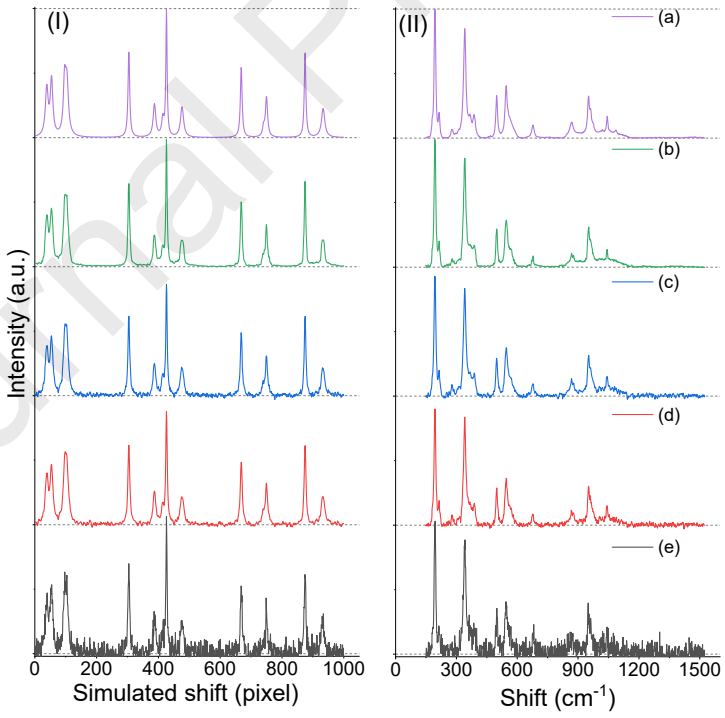

Fig. 2. An example of (I) simulated Raman spectra and (II) experimental Raman spectra of aegirine from the RRUFF project [19] including the (a) original spectrum, the (e) noise-degraded spectrum, and the restored spectrum using different methods,

including (b) MNLM filtering (c) Gaussian filtering (d) median filtering. The noise level is σ_n =0.05, and the frame number is 5, indicating that the original signal is added to 5 different noise vectors, simulating the acquisition of 5 frames of signals with the same parameters. The spectra shown are all 5-frame averaged. The smoothing factor $h = 0.2\sigma_n$, i.e., $k = 0.2$, and the length of searching window w is 30 pixels.

To validate the hypothesis made at the beginning of this paper that applying NLM within multiple frames could help with cancelling unwanted noise, the mean squared error (MSE) against the frame number N is calculated. After generating 30 sets of the original signals, a group of N frames of noise is generated and added to each set of the original signal. So, for each specific original signal, there are N frames of corresponding degraded signal, simulating the Raman spectrum acquired N times from a specific sample. For each set of signal data, averaging, averaging after Gaussian filtering, and averaging after MNLM are conducted, and then compared to the original signal to obtain the MSE. After repeating this process for all 30 sets of data, the average MSE is obtained and shown in Fig. 3(a), vs the number of frames, N, used. Accordingly, the same processing has applied to the experimental dataset, and is shown in Fig. 3(b). MNLM consistently outperforms the other methods when the frame number is greater than 1, which clearly indicates that our assumption is valid. By restoring pixels through averaging based on similarity across different frames, noise cancellation performance is enhanced. Fig. 3 shows that more frames create smaller MSE but cost more time in practice. Fig. 3 also shows 5 frames are already enough for MNLM to produce good results so frame number N is fixed to 5 for further validation.

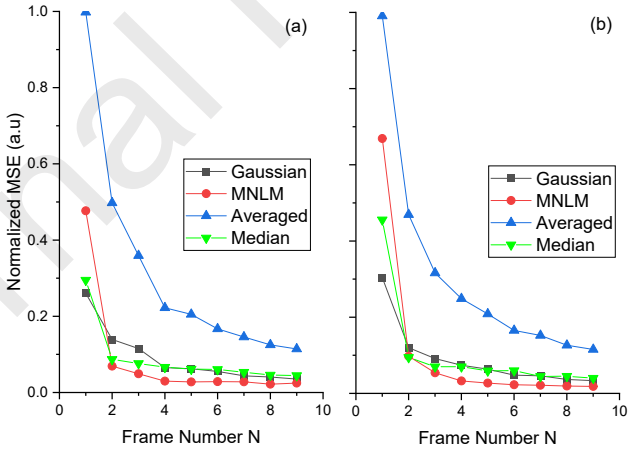

Fig. 3 Average of normalized mean square error (MSE) of restored data with increasing number of frames used. (a) Simulated spectra (b) experimental spectra. The smoothing factor $h = 0.2\sigma_n$, and the length of searching window in each frame, w, is 30 pixels. Standard deviation of the additive noise $\sigma_n = 0.2$. MSE is normalized to σ_n^2

3.2. Parameter sweeping

Having shown the superior effectiveness for both experimental and simulated spectra with fixed denoising parameters, the next imperative step is to find the optimal values of the parameters k and w via parameters sweeping. The parameter sweeping is conducted on simulated datasets as Section 3.1 shows that the effectiveness of our MNLM remains consistent for both experimental and simulated spectra. However, simulated spectra have the advantage of being noise-free, ensuring accurate MSE calculation.

As mentioned in the introduction, some advanced filters, such as SG and WTF, suffer from complicated and sensitive parameter setting which limits their application. In contrast, only two parameters: the length of searching window w and smoothing factor h need to be set for NMLM. Ref. [17] indicated that the denoising results are weakly sensitive to the values of these parameters for NLM. There, the length of the searching window is around 20~30 pixels and smoothing factor is related to the noise, i.e., $h = k\sigma_n$, where the k value is around 0.5 [17]. It is expected that the performance of the MNLM will also be tolerant to variation in these parameters. Therefore, parameter-sweeping for k and w was conducted, and the result is shown in Fig. 4. The k value is within the range from 0.1 to 1 while the w is from 3 to 30 pixels. As shown in Fig. 4, the MSE values for the denoised results are consistently within a range of 0.8×10^{-4} to 1.7×10^{-4}. In the majority of instances, the MSE hovers around 1×10^{-4}, except for certain extreme $k - w$ combinations, e.g. (k~0.1, w~3) and (k~1, w~30). It is evident that the weak sensitivity to parameters has been inherited by MNLM, making it a potential parameter-free denoising method for wider application.

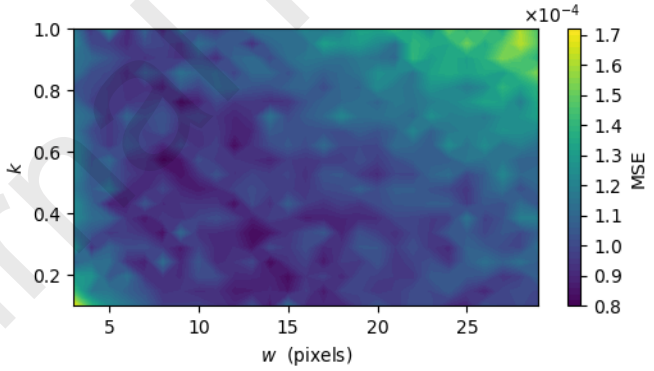

Fig. 4. MSE as function of NMLM parameter k and the length of the search window, w. The frame number N is 5; $\sigma_n = 0.05$.

As illustrated in Fig. 4, there is a discernible trend that the optimal k value tends to decrease with increasing w. However, certain $k - w$ combinations are able to guarantee effective denoising performance in practice. Notable examples include (k~0.6 w~10), (k~0.3 w~20) and (k~0.2 w~30). To enhance applicability in practice, a quick parameter sweeping can be conducted with a standard analyte to characterize the specific spectroscopic devices for optimized parameters setting.

Noting that the smoothing factor $h = k\sigma_n$, considering the standard deviation of noise σ_n could be inaccurately estimated, we fixed $h = 0.01$ and $w = 30$ for subsequent validations regardless the varying noise level, to showcase the effectiveness and robustness of MNLM.

3.3. Statistical indicators

A detailed comparison is presented in Table 1 for simulated spectra dataset and Table 2 for experimental spectra dataset to thoroughly validate the performance of denoising using different denoising methods, including Gaussian and median filtering, under various levels of noise. The noise matrix is generated with different standard deviations (σ_n= 0.05, 0.1, 0.2 and 0.3) and denoising is processed using Gaussian filtering, median filtering, and MNLM filtering. The parameters for the MNLM filtering are kept unchanged (w is 30 pixels, and h is fixed to 0.01, simulating that the user inaccurately estimates the noise level.) to test the robustness of the method without tailoring the parameters to the specific data, while the other two filters are tested with four different filtering parameters each. Specifically, for the Gaussian filtering, the parameter k (i.e., the standard deviation for the Gaussian kernel) is tested for k= 0.1, 0.5, 1, and 2, and for the median filter, the parameter k (i.e., the size of the filter window) is tested for k= 3, 5, 7, and 9. Therefore, for both simulated and experimental spectra datasets, each set of data contains 5 frames of the same signal polluted with random noise of same standard deviations σ_n. Each set of the signal spectrum is then processed with the aforementioned filters, and the restored signal is averaged for comparison with the original signal, to obtain indicators including signal - noise-ratio (SNR), peak signal noise ratio (PSNR), and MSE. After obtaining these indicators for the all spectra sets, the value of each indicator for each filter and averaged signal with noise is averaged and recorded in Table 1 and Table 2 for simulated and experimental dataset, respectively.

Table 1 and Table 2 show the indicators of restored signal from Gaussian filtering and median filtering with different parameters for different-level noise, meanwhile the indicators from MNLM with fixed parameters. It is clearly shown that the performance of each filter varies with the noise level and filtering parameters. However, the MNLM with fixed parameters outperforms all other filters, regardless of the noise level. The other two indicators, including the SNR ratio and PSNR, were also calculated. Thus, after validation with different indicators and comparisons, MNLM has demonstrated outstanding performance and robustness, making it ready for application to practical Raman spectra.

Filter	$*p$	$\sigma_n = 0.05$			$\sigma_n = 0.1$			$\sigma_n = 0.2$			$\sigma_n = 0.3$		
		(a)	(b)	(c)	(a)	(b)	(c)	(a)	(b)	(c)	(a)	(b)	(c)
	10	13.0	32.9	0.51	7.3	27.1	1.95	1.2	21.0	7.98	-3.0	17.5	17.72

G	0.5	14.7	34.6	0.35	9.2	29.0	1.25	3.0	22.8	5.26	-1.1	19.3	11.67
	1	**16.2**	**36.2**	**0.25**	**12.3**	**32.2**	**0.61**	6.2	26.0	2.53	2.1	22.6	5.54
	2	13.3	33.2	0.50	12.1	31.9	0.66	**7.8**	**27.7**	**1.73**	**4.3**	**24.8**	**3.31**
M	3	**15.0**	**35.0**	**0.32**	**11.5**	**31.3**	**0.74**	6.1	25.9	2.57	2.5	22.9	5.09
	5	10.4	30.4	0.95	9.4	29.3	1.24	**6.9**	**26.7**	**2.20**	**5.0**	**25.5**	**2.95**
	7	6.6	26.5	2.30	5.7	25.6	2.90	4.0	23.8	4.34	2.6	23.1	5.23
	9	3.4	23.3	4.86	2.5	22.3	6.32	1.2	21.0	8.64	0.4	20.9	8.99
MN	/	**19.7**	**39.6**	**0.11**	**15.3**	**35.1**	**0.32**	**9.7**	**29.5**	**1.15**	**5.6**	**26.1**	**2.52**
Avg.	/	13.0	32.9	0.51	7.3	27.1	1.95	1.2	21.0	7.98	-3.0	17.5	17.72

Table 1. Indicators for the recovered signal with the best performance for each filter for the simulated spectra dataset, including Gaussian (G), Median (M) and MNLM (MN) with $w = 30, h = 0.01$, and noise level ($\boldsymbol{\sigma_n}$) in bold. (a) signal noise ratio (b) peak signal noise ratio and (c) Mean square error (the value shown in the table is 1000 times MSE). The recovered signal with the best performance for each filter and noise level in bold. *The filter parameter $\boldsymbol{p}$ corresponds to the standard deviation of Gaussian filtering and the window size of Median filtering, respectively. The last line shows the averaged signal.

Filter	$\boldsymbol{p}$	$\boldsymbol{\sigma_n = 0.05}$			$\boldsymbol{\sigma_n = 0.1}$			$\boldsymbol{\sigma_n = 0.2}$			$\boldsymbol{\sigma_n = 0.3}$		
		(a)	(b)	(c)	(a)	(b)	(c)	(a)	(b)	(c)	(a)	(b)	(c)
	10	14.9	33.1	0.49	8.8	27.0	2.00	2.9	21.0	7.91	-0.7	17.4	18.03
G	0.5	16.9	35.0	0.31	10.6	28.8	1.32	4.9	23.1	4.93	1.1	19.3	11.77
	1	**20.1**	38.2	**0.15**	13.7	31.9	0.65	8.7	26.9	2.04	4.6	22.8	5.27

M	2	20.1	**38.3**	0.17	**15.4**	**33.6**	**0.45**	**11.6**	**29.7**	**1.07**	**7.4**	**25.5**	**2.82**
	3	**18.5**	**36.7**	**0.22**	**12.9**	**31.1**	**0.79**	8.0	26.1	2.46	4.7	22.9	5.19
	5	15.3	33.5	0.48	12.4	30.6	0.95	**9.3**	**27.5**	**1.97**	**7.3**	**25.4**	**3.25**
	7	11.0	29.1	1.32	9.0	27.1	2.10	6.4	24.6	3.92	4.9	23.1	5.78
	9	6.6	24.8	3.57	5.2	23.3	5.07	3.1	21.2	8.50	1.9	20.1	11.32
MN	/	**21.5**	**39.6**	**0.12**	**16.8**	**34.9**	**0.34**	**12.2**	**30.3**	**0.99**	**8.4**	**26.5**	**2.30**
Avg.	/	14.9	33.1	0.49	8.8	27.0	2.00	2.9	21.0	7.91	-3.0	17.5	17.72

Table 2. Indicators for the recovered signal with the best performance for each filter for simulated spectra dataset, including Gaussian (G), Median (M) and MNLM (MN) with $w = 30, h = 0.01$, and noise level ($\boldsymbol{\sigma_n}$) in bold. (a) signal noise ratio (b) peak signal noise ratio and (c) Mean square error (Value shown in the table is 1000 times MSE). The recovered signal with the best performance for each filter and noise level in bold. The last line shows the averaged signal.

3.4. Processed experimental spectra comparison.

To validate the MNLM with experimental data in practice, Raman spectra for benzyl alcohol (BnOH) and its deuterated form (d7- BnOH) were obtained using our experimental low-cost WERS system [16]. A measured baseline Raman spectrum for benzyl alcohol was obtained using a conventional Raman microscope. Firstly, the min-max normalization is applied to the Raman spectra from WERS within the region of interest. Following baseline removal, denoising of the WERS spectrum was carried out with MNLM as described above maintaining the same parameters. The denoising processes were conducted with MNLM and baseline filtering methods for comparison. After denoising, a blind deconvolution [22] was conducted to increase the resolution that degraded by the instrument function of the WERS system. Denoising processing typically has a reverse effect to deconvolution, as denoising involves blurring effect at eliminating high-frequency noise, consequently leading to reduction in resolution. Moreover, it is well known that deconvolution is an ill-conditioned process, any noise and inaccuracy during processing can easily cause artefacts or distortion when performing deconvolution [22]. However, as shown in Fig. 5, some fine structures measured using the Raman microscope have been recovered. For example, the multi-peaks in Fig. 5 (I) for BnOH around 1000 cm^{-1} and 1300 $cm^{-1}$and the very small peak around 3100 cm^{-1} have been recovered without causing obvious ringing artifact with MNLM. In contrast with the MNLM, both Gasussian and median filtering result in artifact peaks around the main peak at 1000 cm^{-1} to BnOH spectra, while the flatness in the non-

peak region is inferior to that processed by MNLM. The visual comparison presented in Fig. 5 (II) distinctly demonstrates the pronounced superiority of MNLM over Gaussian and median filtering in restoring the d7-BnOH spectrum. MNLM provides precise denoising so that the fine structures, including tiny multi peaks at 1100 cm^{-1}, 1600 cm^{-1} and 2200 cm^{-1} have all been recovered, while these features are entirely lost with both Gasussian and median filtering.

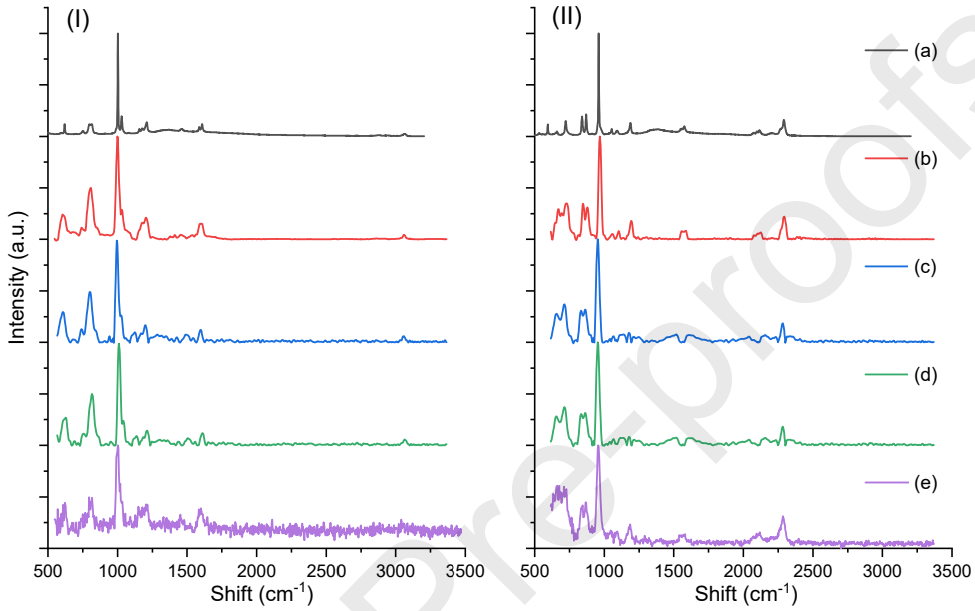

Fig. 5. Raman spectra for (I) benzyl alcohol and (II) its deuterated form d7-benzyl alcohol from (a) a Raman microscope, (b) the processed experimental WERS spectrum via MNLM with $w = 30, h = 0.01$ (c) the processed experimental WERS spectrum with Gaussian filtering (standard deviation is 1) (d) the processed experimental WERS spectrum with median filtering (window size is 3 pixels), and (e) the experimental WERS measurement. Spectra are normalized and shifted for clarity.

4. Conclusion

In summary, a novel MNLM filter has been developed and implemented, enabling the use of information across different frames and applicable to 1D signals. Non-local filtering is more robust than classical conventional neighbour pixels-based approaches such as Gaussian and median filtering. This feature has been extended to multi-frame-based 1D signal denoising. Both statistical indicators for the quality of the restored artificial signal and experimental data processing have demonstrated the excellent performance of our MNLM filter. By applying our MNLM technique, fine structures and subtle Raman features from our WERS system are successfully restored, achieving results comparable to expensive Raman microscopes. This is particularly significant as the WERS, a cost-effective yet recently renewed Raman spectroscopy technique, suffers from strong background and limited resolution. The denoising performances have shown to be insensitive to filter parameters, addressing a limitation of current Raman denoising methods. This attribute is especially beneficial for non-expert users and has the potential

to enable fully automated Raman signal processing. Additionally, it is possible to expand the application to other kinds of 1D optical signals, such as infrared absorption spectra.

Funding. Engineering and Physical Sciences Research Council (EP/R011230/1).

Acknowledgements. Z.L. acknowledges financial support from the China Scholarship Council (201808430227), and B.M.B thanks the Defence Science and Technology Laboratory (DSTLX-1000128554).

Data availability. Data and source code underlying the results presented in this paper are available in Ref. [20]

References list

[1] R. Gautam, S. Vanga, F. Ariese, S. Umapathy, Review of multidimensional data processing approaches for Raman and infrared spectroscopy, EPJ Techn Instrum. 2 (2015) 8. https://doi.org/10.1140/epjti/s40485-015-0018-6.

[2] N. Le Thomas, A. Dhakal, A. Raza, F. Peyskens, R. Baets, Impact of fundamental thermodynamic fluctuations on light propagating in photonic waveguides made of amorphous materials, Optica. 5 (2018) 328. https://doi.org/10.1364/optica.5.000328.

[3] A. Kumar, S.S. Sodhi, Comparative analysis of gaussian filter, median filter and denoise autoenocoder, in: 2020 7th International Conference on Computing for Sustainable Global Development (INDIACom), IEEE, 2020: pp. 45–51.

[4] P.M. and K.V. Martin Clupek, Noise reduction in Raman spectra: Finite impulse response filtration versus Savitzky–Golay smoothing, Journal of Raman Spectroscopy. 38 (2007) 1538–1553. https://doi.org/10.1002/jrs.

[5] H. Chen, W. Xu, N. Broderick, J. Han, An adaptive denoising method for Raman spectroscopy based on lifting wavelet transform, Journal of Raman Spectroscopy. 49 (2018) 1529–1539. https://doi.org/10.1002/jrs.5399.

[6] X.Y. Zhao, G.Y. Liu, Y.T. Sui, M. Xu, L. Tong, Denoising method for Raman spectra with low signal-to-noise ratio based on feature extraction, Spectrochimica Acta Part A: Molecular and Biomolecular Spectroscopy. 250 (2021) 119374. https://doi.org/10.1016/j.saa.2020.119374.

[7] G. Zhang, H. Hao, Y. Wang, Y. Jiang, J. Shi, J. Yu, X. Cui, J. Li, S. Zhou, B. Yu, Optimized adaptive Savitzky-Golay filtering algorithm based on deep learning network for absorption spectroscopy, Spectrochimica Acta Part A: Molecular and Biomolecular Spectroscopy. 263 (2021) 120187. https://doi.org/10.1016/j.saa.2021.120187.

[8] A.R. Ferreira da Silva, Wavelet denoising with evolutionary algorithms, Digital Signal Processing. 15 (2005) 382–399. https://doi.org/10.1016/j.dsp.2004.11.003.

[9] J. Hu, D. Zhang, H. Zhao, B. Sun, P. Liang, J. Ye, Z. Yu, S. Jin, Intelligent spectral algorithm for pigments visualization, classification and identification based on Raman spectra, Spectrochimica Acta Part A: Molecular and Biomolecular Spectroscopy. 250 (2021) 119390. https://doi.org/10.1016/j.saa.2020.119390.

[10] A. Buades, B. Coll, J.-M. Morel, A Non-Local Algorithm for Image Denoising, in: 2005 IEEE Computer Society Conference on Computer Vision and Pattern Recognition (CVPR'05), IEEE, San Diego, CA, USA, 2005: pp. 60–65. https://doi.org/10.1109/CVPR.2005.38.

[11] J. Froment, Parameter-Free Fast Pixelwise Non-Local Means Denoising, Image Processing On Line. 4 (2014) 300–326. https://doi.org/10.5201/ipol.2014.120.

[12] P. Jain, V. Tyagi, A survey of edge-preserving image denoising methods, Inf Syst Front. 18 (2016) 159–170. https://doi.org/10.1007/s10796-014-9527-0.

[13] Y. Lv, Q. Zhu, R. Yuan, Fault Diagnosis of Rolling Bearing Based on Fast Nonlocal Means and Envelop Spectrum, Sensors. 15 (2015) 1182–1198. https://doi.org/10.3390/s150101182.

[14] A. Buades, B. Coll, J.M. Morel, A Review of Image Denoising Algorithms, with a New One, Multiscale Model. Simul. 4 (2005) 490–530. https://doi.org/10.1137/040616024.

[15] X. Fan, Y. Zeng, Y. Zhi, T. Nie, Y. Xu, X. Wang, Signal-to-noise ratio enhancement for Raman spectra based on optimized Raman spectrometer and convolutional denoising autoencoder, J Raman Spectroscopy. 52 (2021) 890–900. https://doi.org/10.1002/jrs.6065.

[16] M.A. Ettabib, B.M. Bowden, Z. Liu, A. Marti, G.M. Churchill, J.C. Gates, M.N. Zervas, P.N. Bartlett, J.S. Wilkinson, Grating-incoupled waveguide-enhanced Raman sensor, Plos One. 18 (2023) e0284058.

[17] A. Buades, B. Coll, J.-M. Morel, Non-Local Means Denoising, in: Image Processing On Line, 2011: pp. 208–212. https://doi.org/10.5201/ipol.2011.bcm_nlm.

[18] P. Virtanen, R. Gommers, T.E. Oliphant, M. Haberland, T. Reddy, D. Cournapeau, E. Burovski, P. Peterson, W. Weckesser, J. Bright, S.J. van der Walt, M. Brett, J. Wilson, K.J. Millman, N. Mayorov, A.R.J. Nelson, E. Jones, R. Kern, E. Larson, C.J. Carey, İ. Polat, Y. Feng, E.W. Moore, J. VanderPlas, D. Laxalde, J. Perktold, R. Cimrman, I. Henriksen, E.A. Quintero, C.R. Harris, A.M. Archibald, A.H. Ribeiro, F. Pedregosa, P. van Mulbregt, SciPy 1.0 Contributors, SciPy 1.0: Fundamental Algorithms for Scientific Computing in Python, Nature Methods. 17 (2020) 261–272. https://doi.org/10.1038/s41592-019-0686-2.

[19] B. Lafuente, R.T. Downs, H. Yang, N. Stone, 1. The power of databases: The RRUFF project, Highlights in Mineralogical Crystallography. (2015) 1–30. https://doi.org/doi.org/10.1515/9783110417104-003.

[20] Z. Liu, Dataset supporting the publication: 'Multiframe-based non-local means denoising for Raman spectra, University of Southampton, (2023). https://doi.org/10.5258/SOTON/D2639.

[21] J. Laumer, S.K. O'Leary, A root-mean-square-error analysis of two-peak Gaussian and Lorentzian fittings of thin-film carbon Raman spectral data, Journal of Applied Physics. 126 (2019) 045706. https://doi.org/10.1063/1.5089139.

[22] T.F. Chan, C.K. Wong, Total variation blind deconvolution, IEEE Transactions on Image Processing. 7 (1998) 370–375. https://doi.org/10.1109/83.661187.

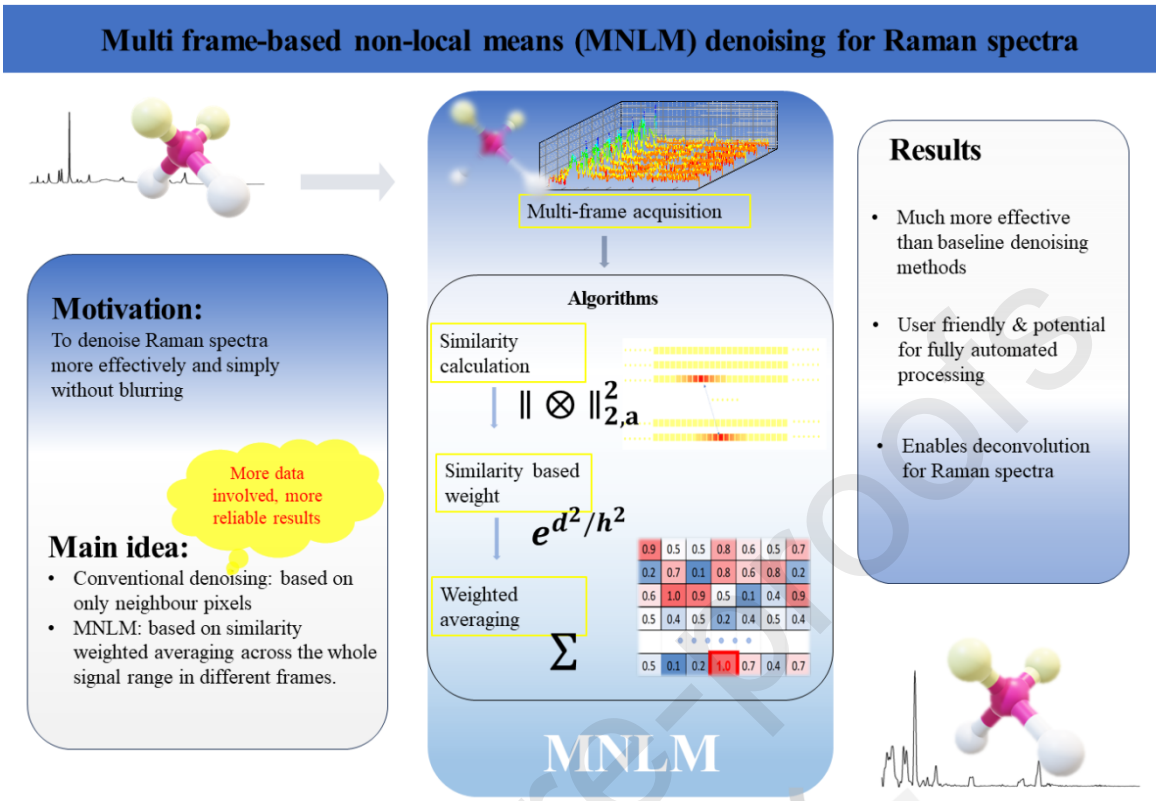

- New mechanism: Exploiting data across different frames to denoise each pixel
- Superior performance: Shown by extensive validations and comparisons
- Weak sensitivity of parameters setting: User-friendly, potential full automation
- High precision denoising: A vital factor that enables successful deconvolution

Zhen Liu: Conceptualization，Methodology，Validation，Formal analysis Writing - Original Draft，Software，Data Curation

Mohamed A. Ettabib: Resources, Data Curation, Supervision

Bethany M. Bowden: Resources, Data Curation

Philip N. Bartlett: Writing - Review & Editing，Project administration，Funding acquisition

James S. Wilkinson: Writing - Review & Editing，Project administration，Supervision，Funding acquisition

Michalis N. Zervas: Writing - Review & Editing，Project administration，Supervision，Funding acquisition

Declaration of interests

☒ The authors declare that they have no known competing financial interests or personal relationships that could have appeared to influence the work reported in this paper.

☐ The authors declare the following financial interests/personal relationships which may be considered as potential competing interests: